Numerical study of an innovative cross-flow turbine

Quentin Clémençot, Pierre-Luc Delafin, Thierry Maître

17èmes JOURNEES DE L'HYDRODYNAMIQUE
JH2020

24 - 26 novembre 2020
CHERBOURG - en - COTENTIN

Numerical study of an innovative cross-flow turbine

Q. Clémençot[(1),*], P.-L. Delafin[(1)], and T. Maître[(1)]

[(1)]Univ. Grenoble Alpes, CNRS, Grenoble INP, LEGI, 38000 Grenoble, France
[*]Corresponding author: quentin.clemencot@univ-grenoble-alpes.fr

Résumé

Un concept de turbine bi-axiale est étudié par simulation numérique. Inspiré du principe des turbines Darrieus, les extrémités des pales de cette turbine sont en liaison cinématique avec une chaîne, elle-même reliée à deux poulies de même rayon. Chaque pale a donc un mouvement de translation dans une direction orthogonale à la vitesse d'écoulement amont sur une partie de sa trajectoire. L'angle d'incidence constant sur ces portions permet d'atteindre des rendements élevés pour une turbine à axe transverse. Les simulations URANS k-ω SST sont réalisées à l'aide de OpenFOAM®v2006. Un maillage dynamique de type overset est mis en place et permet d'imposer la cinématique de la pale. Une validation du procédé de simulation est faite par comparaison avec des données expérimentales et numériques d'un cas d'aile oscillante. L'influence de la solidité sur le coefficient de puissance moyen et instantanné est étudiée pour des turbines mono-pale, ce qui revient à étudier l'influence de la longueur de corde. Lorsque la solidité augmente, la vitesse optimale d'entraînement de pale diminue et le Cp instantané maximal augmente.

Summary

A bi-axial turbine concept is studied by numerical simulation. Inspired by the principle of Darrieus turbines, the tips of the blades of this turbine are kinematically linked to a chain, itself connected to two pulleys of the same radius. Each blade thus has a translational movement in a direction orthogonal to the upstream flow speed over part of its trajectory. The constant angle of attack on these portions makes it possible to achieve high efficiencies for a cross flow turbine. URANS k-ω SST simulations are performed using OpenFOAM®v2006. A dynamic overset type mesh is set up to impose the kinematics of the blade. A validation of the simulation process is made by comparison with experimental and numerical data of an oscillating airfoil case. The influence of solidity on the mean and instantaneous power coefficients is studied for one-blade turbines, which amounts to studying the influence of the chord length. As the solidity increases, the optimal blade drive speed decreases and the maximum instantaneous Cp increases.

1. Introduction

Vertical axis turbines have been widely studied in recent decades [1, 2, 3, 4]. However, the efficiency obtained with Darrieus turbines seem to be intrinsically limited by their design. It is therefore interesting to imagine a new concept of vertical axis turbine that would be able to approach or even surpass the performances of horizontal axis turbines. A new type of double-axis cross-flow turbine is being investigated here. This design allows a perpendicular translation of the blades with respect to the upstream velocity on two portions of the

trajectory (see Figure 1). Naccache and Paraschivoiu have worked on this concept using URANS simulations and showed the potential of the turbine [5]. With a single blade and a zero setting angle (the angle between the chord and the blade trajectory), they obtained a power coefficient CP $= 0.4$ from a 3D simulation. The optimization of the turbine parameters, including the introduction of a new blade orientation law, should make it possible to exceed these performances, which are already comparable to the best Darrieus turbines. The aim of the present work is to study the effect of solidity on the performance of such a turbine.

2. Turbine Specification

2.1 Main characteristics

As the name implies, the bi-axial turbine has two distinct axes of rotation perpendicular to the upstream flow velocity vector (Figure 1). A system of pulleys and chains connects the upper and lower axes to each other. The blades are symmetrical NACA0012 profiles. They are placed at regular intervals along these chains. Therefore, during one cycle, a blade performs a downward vertical translation, half a revolution around the lower axis, an upward vertical translation and then, half a revolution around the upper axis. Along the translation parts, the angle of attack is near to be constant (if we assume a uniform incoming flow and neglect the wake effects of the other blades). This characteristics should allow this turbine design to reach higher efficiencies than a conventional Darrieus turbine. It can be noted that in the case $h = 0$, the turbine is equivalent to a Darrieus turbine.

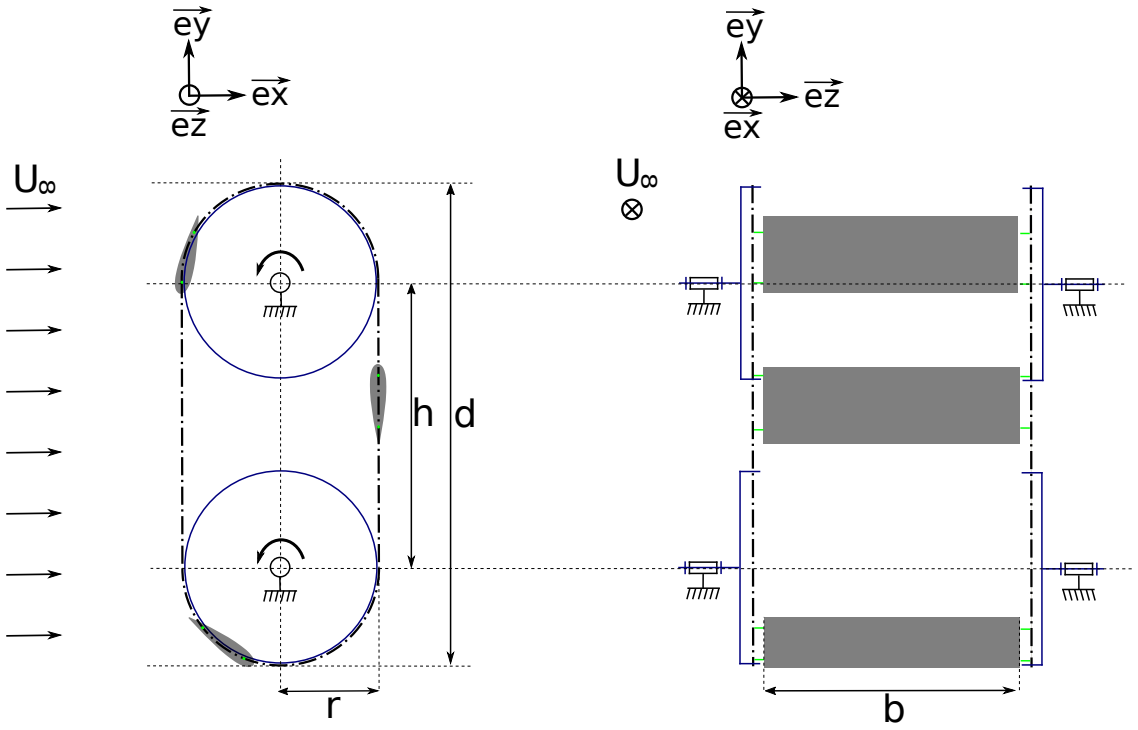

Figure 1. Scheme of a 3-blade turbine with a side (left) and front (right) views. The turbine studied in this article has only one blade.

2.2 Description of motion

Each tip of a blade has two points of connection with the chain (Figure 2). Point A near the leading edge is connected to a chain link with a (A,$\vec{e_z}$)-axis pivot. Point B near the trailing edge has a kinematic link with a chain link which allows rotation of axis (B,$\vec{e_z}$) and translation tangent to the chain. Points A and B belong to the chord line and have the same trajectory. In this study, the parameters $x_a = 1/8$ and $x_b = 7/8$ are constant. Their influence on the turbine performance will be studied in the future. The speed of the chain, $V = \omega * r$

with $\vec{\omega} = \omega.\vec{e_z}$ the rotational speed of the pulleys, is constant. The parameter $\lambda = V/U_\infty$ is defined by analogy with the tip speed ratio (TSR) of horizontal axis turbines: it is the ratio between the blade speed and the far field flow velocity.

By convention, the origin of the fixed coordinate frame R_0=($\vec{e_x}$,$\vec{e_y}$,$\vec{e_z}$) is taken at the centre of the upper pulley. $\vec{e_x}$ has the same direction as the far field velocity vector. The $\vec{e_y}$ vector belongs to the study plan and points in the upward direction. A local reference frame ($\vec{e_t}$,$\vec{e_n}$,$\vec{e_z}$) is defined centred at point A (Figure 2). The vector $\vec{e_t}$ is tangent to the point trajectory and the vector $\vec{e_n}$ is normal to this trajectory. This local reference frame will be used to project the hydrodynamic forces as well as to write the velocity vector of the centre of rotation of the blade.

The following angles are defined :

- γ : angle between the downstream direction, $\vec{e_x}$, and the tangent to the trajectory at point A, $\vec{e_t}$.
- θ : angle between $\vec{e_x}$ and the chord line ($\vec{BA}$ vector more specifically)
- β : the setting angle defined as the angle between the tangent to the trajectory at point A, $\vec{e_t}$, and the chord line.

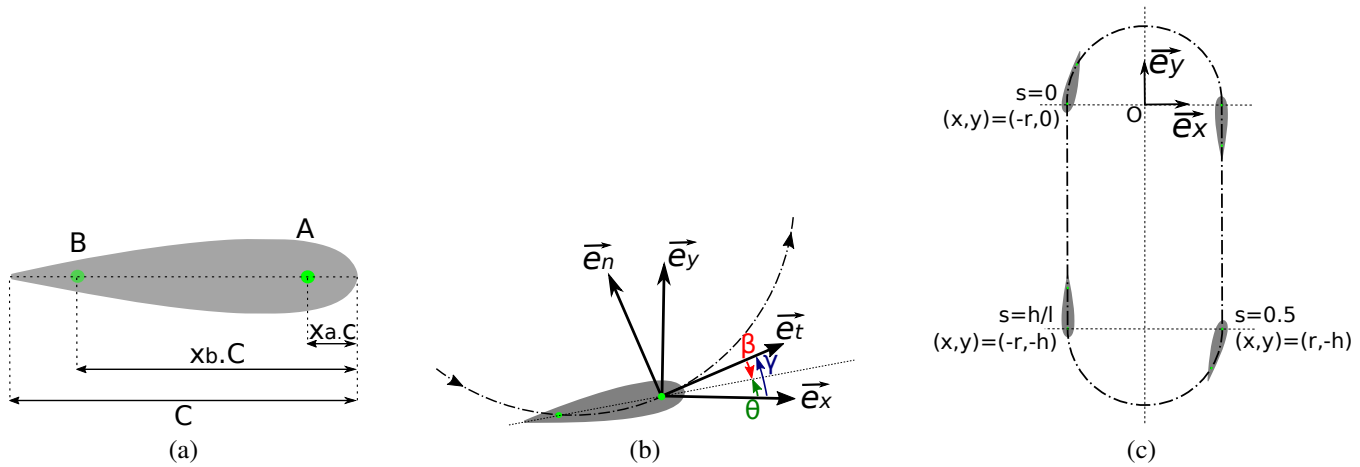

Figure 2. Position of contact points A and B between blade and chain (a), definition of angles and reference frames (b) and position parameter s (c).

A position parameter, noted “s” and varying from 0 to 1, is introduced (Figure 2). It enables to locate the centre of rotation A along its trajectory. By convention, $s = 0$ when attachment point A starts its downward translation. Thus, the position, velocity and acceleration of point A can be seen as a function of s (Figure 3).

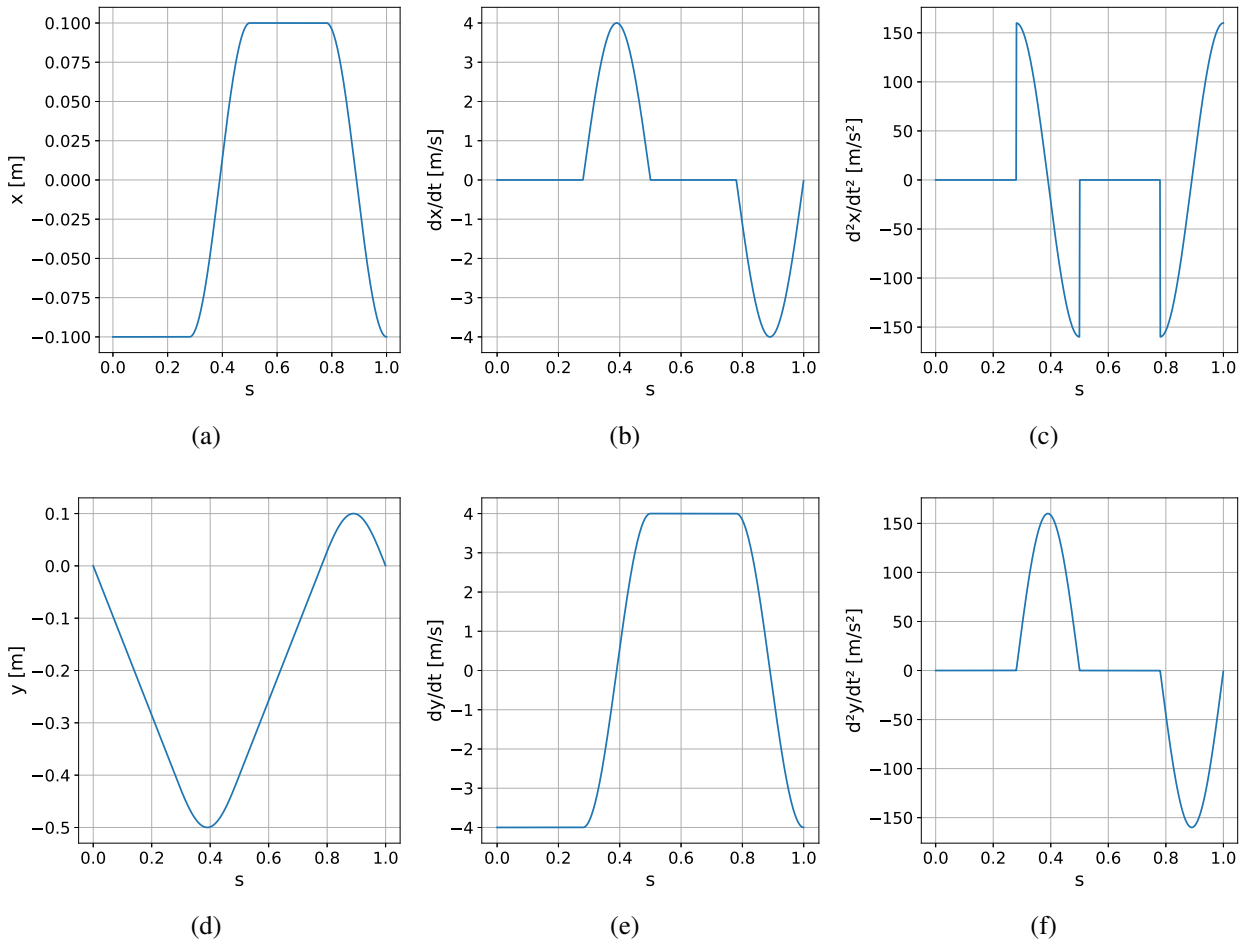

Figure 3. Position, velocity and acceleration in $\vec{ex}$ and $\vec{ey}$ of attachment point A as a function of position parameter s for $h = 0.4$m, $r = 0.1$m and $V = 4$m/s.

Depending on the position of points A and B along their trajectory, the blade is either in vertical translation, in rotation around one of the pulley axes or in transition between these two states, i.e. a motion composed of a rotation and a translation (Figure 4).

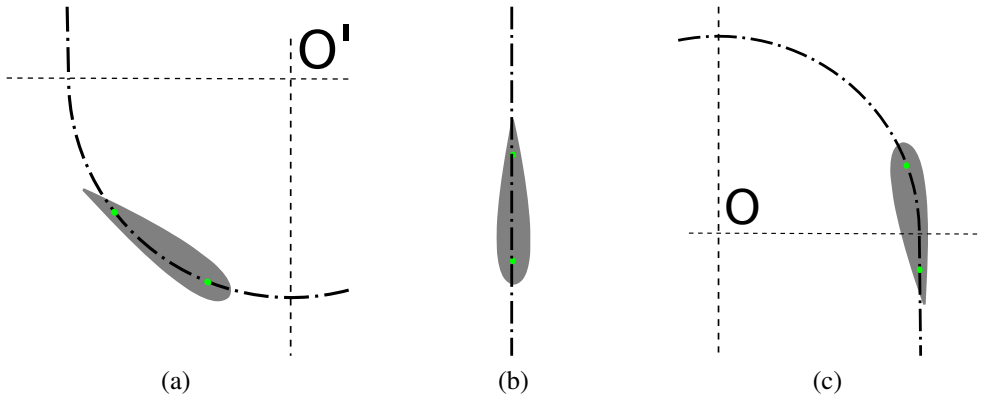

Figure 4. Examples of three kinematic states of the blade : a pure rotation around the lower pulley axis (a), a pure translation (b) and a composite kinematics of translation and rotation (c).

2.3 Advantage of this kinematics

Other kinematics are conceivable for the blades. For example, it is possible to consider a case where a blade is fixed to a single chain link. The chord line would always be tangent to the blade trajectory, so the setting angle would be constant and equal to 0. The kinematics of the blade would be easier to describe with only two possible states: a vertical translation or a rotation around a pulley. There will be no more transition between translation and rotation. But with such a model, the speed of rotation is a discontinuous function of the position parameter and therefore of time. Indeed, at the end of the translation, the rotational speed of the blade passes instantaneously from $d\theta/dt = 0$ to $d\theta/dt = \omega$ and returns instantaneously to $d\theta/dt = 0$ at the end of the rotation (Figure 5). A discontinuous angular velocity implies a theoretically infinite acceleration and forces. In practice, the blades would be subject to high mechanical stresses four times per revolution, resulting in premature material fatigue.

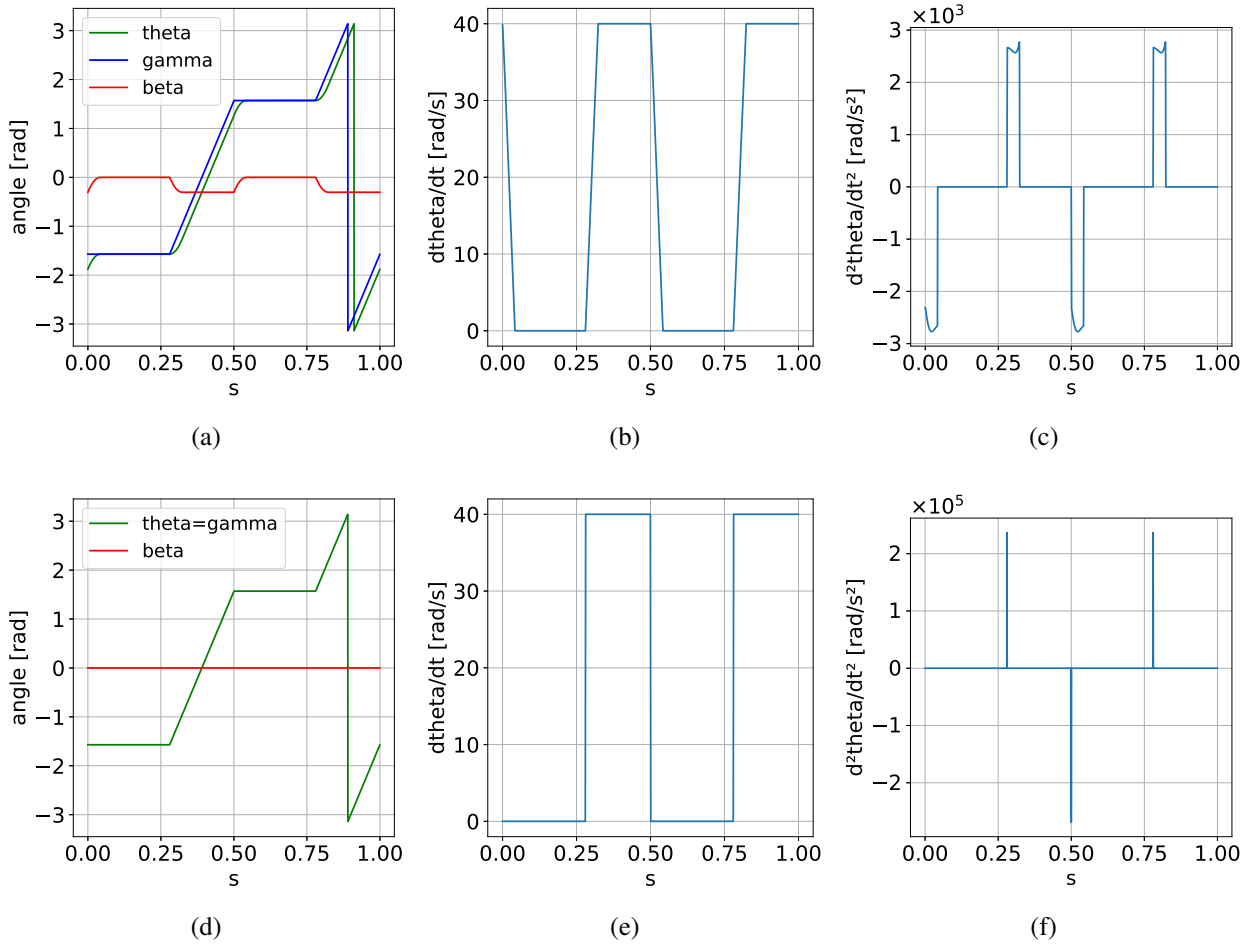

Figure 5. Angular position, angular velocity and angular acceleration of a blade as a function of its position for 2 turbine configurations. The upper figures correspond to a configuration with two points A and B of connection between the blade and the chain with $x_a = 1/8c$ and $x_b = 7/8c$. The lower figures correspond to a configuration with a blade attached to the chain at a single point located $1/8c$ away from the leading edge. For both cases, we take h=0.4m, r=0.1m, V=4m/s, c=0.08m.

2.4 Power extraction

Considering the blade as a non-deformable solid, its kinematic torsor can be written at point A in the fixed reference frame $\mathscr{R}$ as a function of time, which gives Equation 1.

$$\{\mathscr{V}_{b/\mathscr{R}}\}(t) = \left\{ \begin{array}{l} \overrightarrow{\omega}_{b/\mathscr{R}}(t) \\ \overrightarrow{V}_{A\in b/\mathscr{R}}(t) \end{array} \right\}_A \tag{1}$$

with $\vec{\omega}_{b/\mathscr{R}}(t) = \omega_{b/\mathscr{R}}(t).\vec{ez}$ the angular velocity of the blade and $\vec{V}_{A\in b/\mathscr{R}}(t) = V.\vec{e_t}(t)$ the velocity of the point A.

Similarly, the torsor of the mechanical action that the fluid exerts on the blade can be written at point A, which gives Equation 2.

$$\{\mathscr{T}_{f\to b}\}(t) = \left\{ \begin{array}{l} \overrightarrow{F}_{f\to b}(t) \\ \overrightarrow{M}_{A,f\to b}(t) \end{array} \right\}_A \tag{2}$$

with $\overrightarrow{F}_{f\to b}(t) = \overrightarrow{F}_t(t).\vec{e_t}(t) + \overrightarrow{F}_n(t).\vec{e_n}$ the force exerted by the fluid on the blade and $\overrightarrow{M}_{A,f\to b}(t) = M_{A,f\to b}(t).\vec{e_z}(t)$ the moment calculated at point A of the action of the fluid on the blade.

To simplify the notations, a time function ϕ at time t will henceforth be noted $\phi(t) = \phi$ and the temporal average of ϕ will be noted $\overline{\phi}$. The power transmitted by the fluid to the blade is written as the product of the kinematic tensor by the mechanical action torsor, both written at the same point (point A is chosen here). The intantaneous power harnessed by a blade is therefore given by Equation 3.

$$P = \overrightarrow{F}_{f\to b}.\overrightarrow{V}_{A\in b/\mathscr{R}} + \overrightarrow{M}_{A,f\to b}.\overrightarrow{\omega}_{p/\mathscr{R}} \tag{3}$$

The instantaneous power coefficient harnessed by a blade is equal to the ratio of P to the kinetic power of the upstream flow passing through an area equal to the area covered by the blade during its revolution, projected in the direction of flow.

$$C_p = \frac{P}{\frac{1}{2}\rho U_\infty^3 db} \tag{4}$$

with ρ the density of the fluid, U_∞ the magnitude of the upstream velocity, b the blade span and d the total height of the turbine. The coefficients of forces in directions $\vec{e_x}$, $\vec{e_y}$, $\vec{e_t}$ and $\vec{e_n}$ as well as a coefficient of moment are defined by Equation 5.

$$C_{x,y,t,n} = \frac{F_{x,y,t,n}}{\frac{1}{2}\rho U_\infty^2 cb} \quad and \quad C_{m_A} = \frac{M_{A,f\to b}}{\frac{1}{2}\rho U_\infty^2 c^2 b} \tag{5}$$

From these definitions, it is possible to rewrite the power coefficient as a function of the force coefficients, resulting in Equation 6.

$$C_p = C_t \times \frac{c}{d} \times \lambda + C_{mA} \times \omega_{b/\mathscr{R}} \times \frac{c^2}{d.U_\infty} \tag{6}$$

Figure 6 shows the C_p obtained with a 1-blade turbine with $h = 0.4$m, $r = 0.1$m, $c = 0.08$m and $\lambda = 4$.

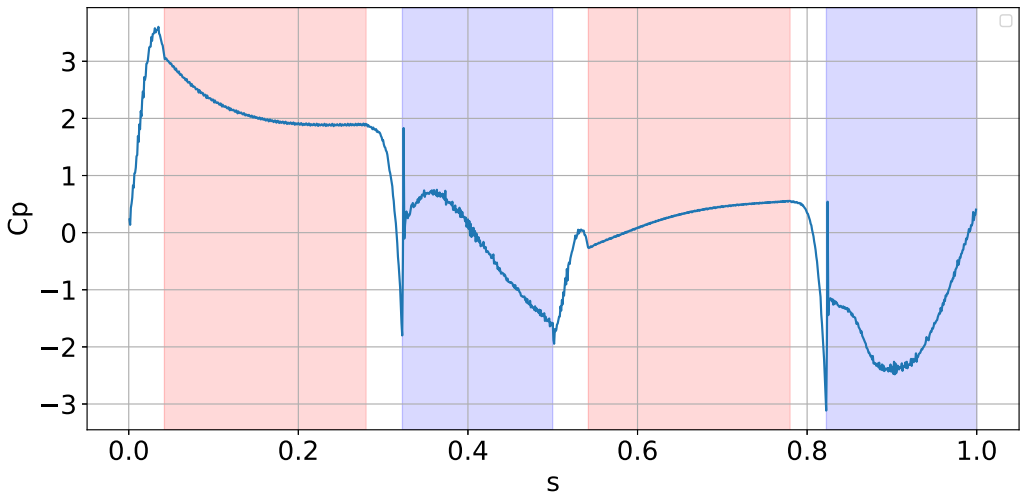

Figure 6. Power coefficient of one blade as a function of its position parameter for $h = 0.4$m, $r = 0.1$m, $c = 0.08$m, $\lambda = 4$. Red areas correspond to the times when the blade is in translation. Blue areas correspond to the moments when the blade is rotating.

3. Numerical simulation

3.1 Numerical solver

Simulations are carried out using OpenFoam®v2006 software. The flow is modelled using the URANS (Unsteady Reynolds-averaged Navier–Stokes) equations and the two-equation k-ω SST turbulence model [6]. The finite volume method with PIMPLE algorithm is used to solve these equations. The PIMPLE algorithm is a combination of PISO (Pressure Implicit with Splitting of Operator) and SIMPLE (Semi-Implicit Method for Pressure-Linked Equations). Time step, computational domain size and mesh sensitivity analyses have been considered and the first cell on the blade was defined so that $y^+ \sim 1$.

3.2 Overset mesh

The presence of moving solids in the simulation domain requires the implementation of a dynamic meshing strategy. An overset meshing technique is used here. A fixed background mesh occupies the entire simulation area. Overset meshes are superimposed on the background mesh and move relative to it. The cells at the border of the overset mesh have a face without neighbouring cells. The value of the fields for these cells cannot be calculated conventionally. There value is therefore interpolated from the background cells on which they are superimposed. Some of the background cells covered by the overset mesh are disabled (they are neither calculated nor interpolated). The cells adjacent to the deactivated cells are interpolated, so there is a two-way transfer of information between the meshes (Figure 7). The overset meshes are independent of each other and their position and orientation can be imposed at each time step, which allows a very high flexibility of use.

In our case, blade is located in the middle of an overset mesh and a multi-block structured O-grid topology is used. The blade is described by 364 cells. The geometry of the boundary of the overset mesh is chosen so that all points of the chord are at the same distance from the overset boundary. This radial distance is the same for all chord lengths. It corresponds to $0.5c$ in the case of a blade with a chord length of 8cm, which is the longest chord tested here (Figure 8). The size of the finest cells of the background is $0.0026d$, which corresponds to $0.02c$ for a blade with an 8cm chord. The ratio between the size of the overset boundary cells and the finest cells in the background is 0.78. It must be close to 1 to have a good interpolation of the fields between the background and the overset. The most refined backgound area over which the overset mesh

moves has a width of $5r$ in the direction of flow and a height of $1.5d$. The size of the simulation domain is large enough to make blocking effects negligible (Figure 8).

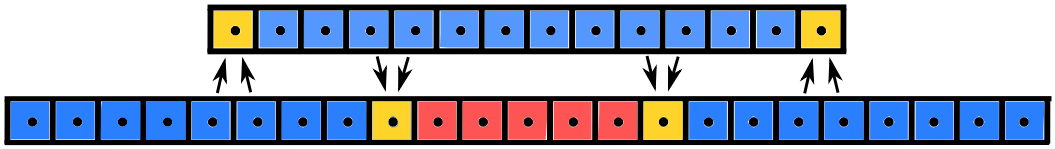

Figure 7. Scheme of an 1D overet mesh (top cell group) and its associated background mesh (bottom cell group).Blue cells are calculated, yellow cells are interpolated and red cells are disabled. The arrows represent the transfer of information from one mesh to another for interpolated cells.

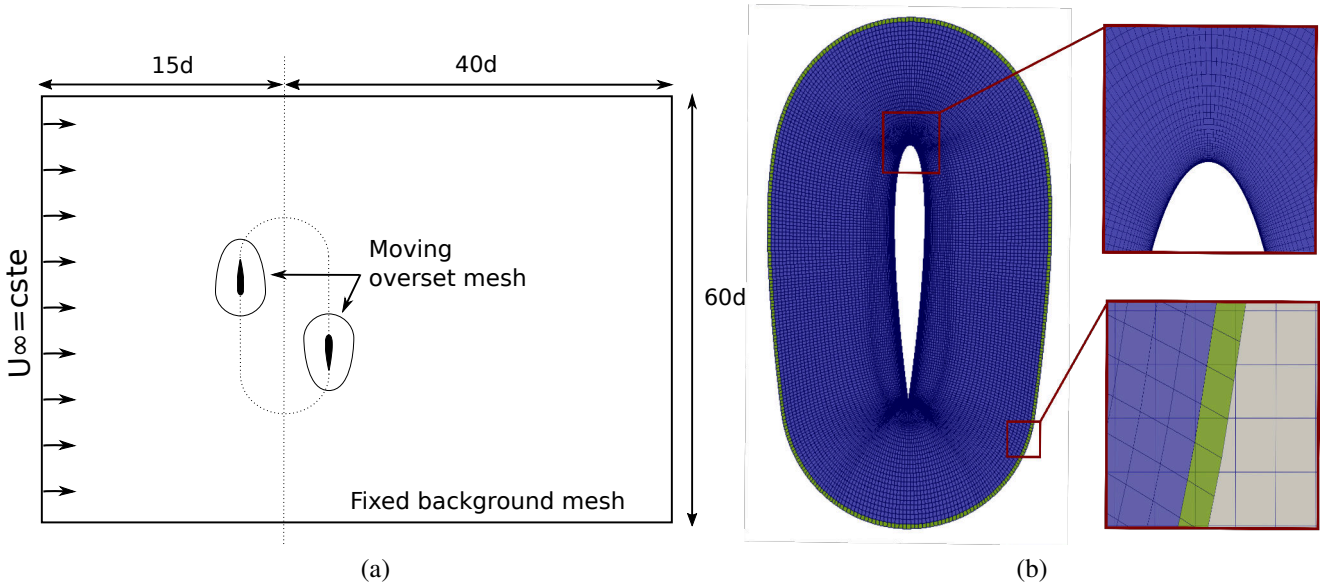

Figure 8. Scheme of the simulation domain and the overset mesh (not to scale) (a) and view of an overset mesh with the calculated cells in blue and the interpolated cells in green (b)

3.3 Validation

Since there are no experimental data on this new type of turbine yet, the validation of the numerical simulation process will be done by comparison with a more classical case of an oscillating airfoil. The case of a NACA0012 profile oscillating in a sinusoidal motion has been extensively studied experimentally and numerically. In this configuration, the airfoil pitch axis is located at 1/4-chord from the leading edge and the instantaneous angle of attack is given by Equation 7.

$$\alpha(t) = \alpha_0 + \Delta_\alpha sin(\omega t) \tag{7}$$

The results of the simulation with overset mesh on a highly dynamic configuration are compared with the experimental results of Lee and Gerontakos [7] and numerical results of Delafin [8] (Figure 9). The relatively good agreement between these results shows that the overset type meshes can be used in the case of a airfoil undergoing a variable angle of attack. This is an interesting point of validation because the blades of the bi-axial turbine studied here see a variable angle of attack in the upper and lower rotations.

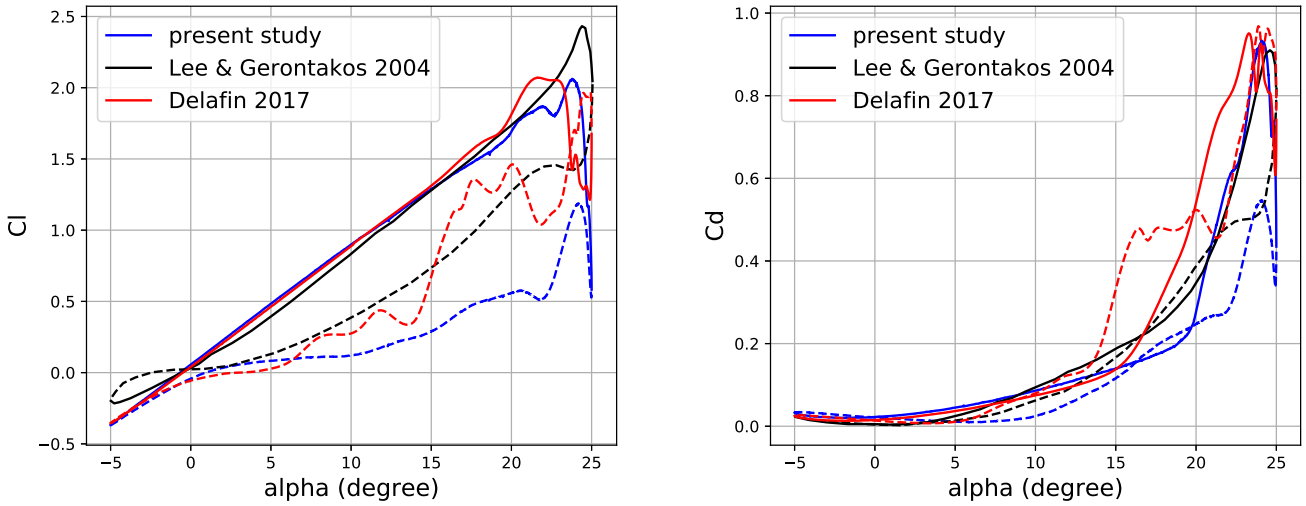

(a) (b)

Figure 9. Force coefficients comparison α(t)=10°+15°$sin(\omega t)$ with k=ωc/2U_∞=0.1 and Re=1.35x10^5. The continuous line corresponds to the increasing AoA and the dashed line corresponds to the decreasing AoA.

4. Results

In this part the performances obtained with single-bladed turbines and different chord lengths will be presented. Therefore, the solidity parameter $\sigma = Nc/(2\pi r + 2h)$ will vary from one case to another.

All other things being equal, the average C_p of the turbine depends on λ. For the same solidity value, several simulations with different λ values were therefore run. A curve of mean C_p versus λ is then plotted, which has a convex shape with an overall maximum expected for optimal λ (Figure 10). Table 1 summarizes the cases tested. It should be noted that the variation in average C_p between two consecutive blade cycles is of the order of 2%. A finer convergence will be necessary to conclude on the performances achievable by this turbine. The general behaviour observed here should however persist.

c [cm]	σ	λ	$\overline{C_p}$
8	0.056	3	0.26
8	0.056	4	0.45
8	0.056	5	0.31
8	0.056	6	-0.19
4	0.028	3	-0.01
4	0.028	4	0.50
4	0.028	5	0.58
4	0.028	6	0.59
2.66	0.0186	4	0.18
2.66	0.0186	5	0.47
2.66	0.0186	6	0.52
2.66	0.0186	7	0.51

Table 1. Summary of the results of average power coefficient ($\overline{C_p}$) obtained at different λ and with different solidities (σ).

As shown in Figure 10, optimal λ increases with decreasing solidity. This is an expected result observed in the case of Darieus turbines [9]. When the blade is in translation, the power harnessed is maximum for a

given angle of attack α_{opt}. When the solidity decreases, the average streamwise velocity inside the turbine increases. The angle of attack seen by the blade therefore also increases. It is then necessary to increase λ, and thus the speed of the blade, to return to α_{opt}.

During translation, the constant angle of attack allows the development of a permanent flow regime and therefore a constant power coefficient. This explains the asymptotes on the C_p curves in Figure 11 and Figure 12. When the blade is rotating around a pulley axis, the angle of attack changes rapidly and will occasionally exceed the stall angle, resulting in dynamic stall and vortex shedding. Figure 13 shows the different flow regimes that a blade encounters during a cycle.

Finally, C_p max as well as the amplitude of the peak at the beginning of the rotation increases with the length of the chord. To limit the mechanical stresses, it would therefore be preferable to reduce the chord size. In order to keep the same solidity parameter, the number of blades will have to be increased.

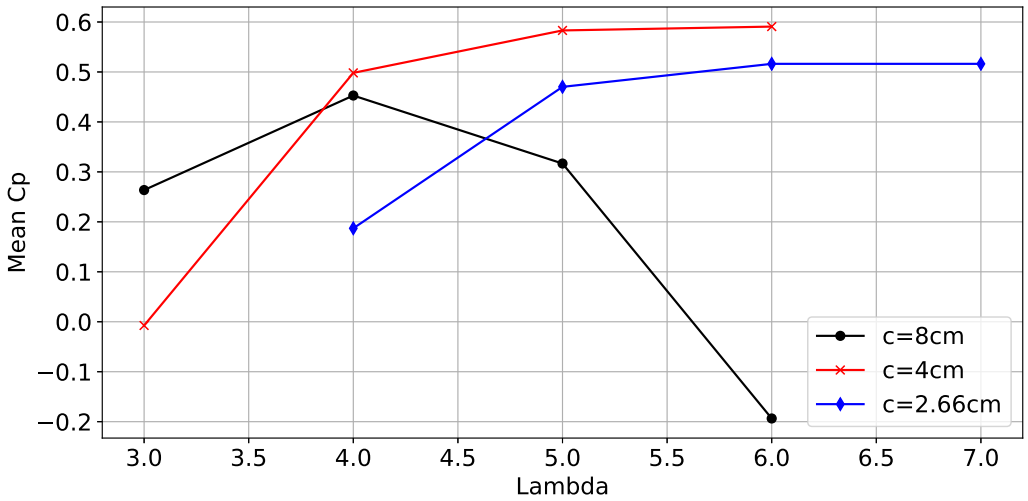

Figure 10. Mean C_p as a function of λ for different chord lengths for 1-blade turbine with $c = 0.04$m, $h = 0.4$m and $r = 0.1$m.

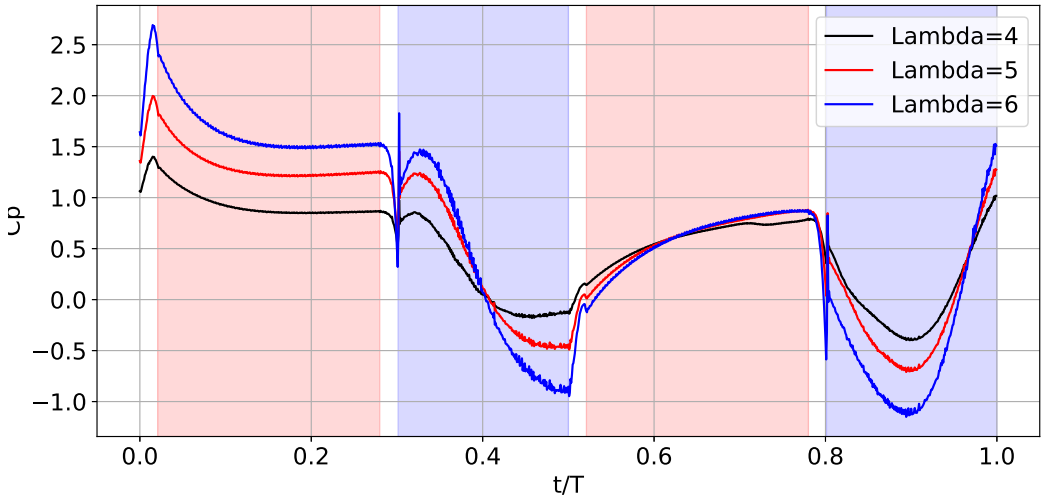

Figure 11. Comparison of instantaneous C_p for different λ for 1-blade turbine with $c = 0.04$m, $h = 0.4$m and $r = 0.1$m for all cases.

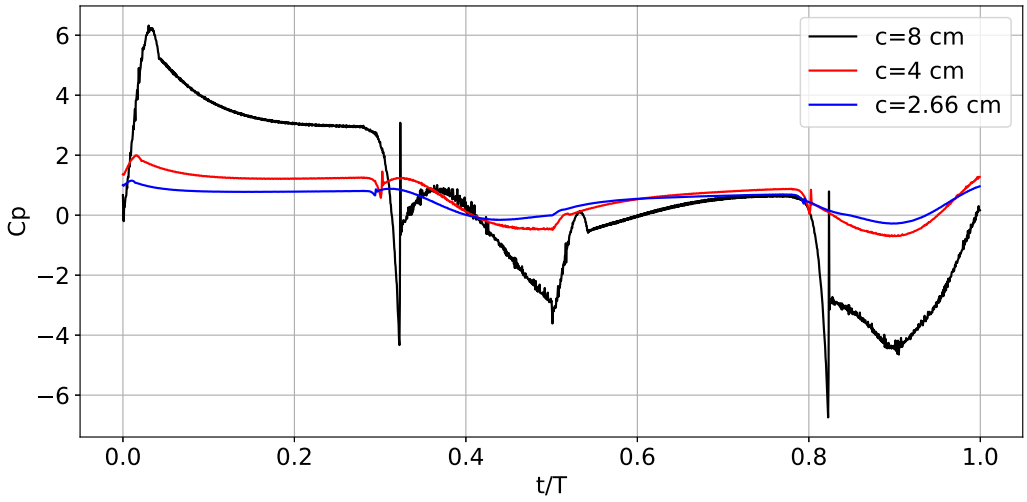

Figure 12. Comparison of instantaneous C_p for different chord lengths for 1-blade turbines with $c = 0.04$m, $h = 0.4$m and $r = 0.1$m and $\lambda = 5$

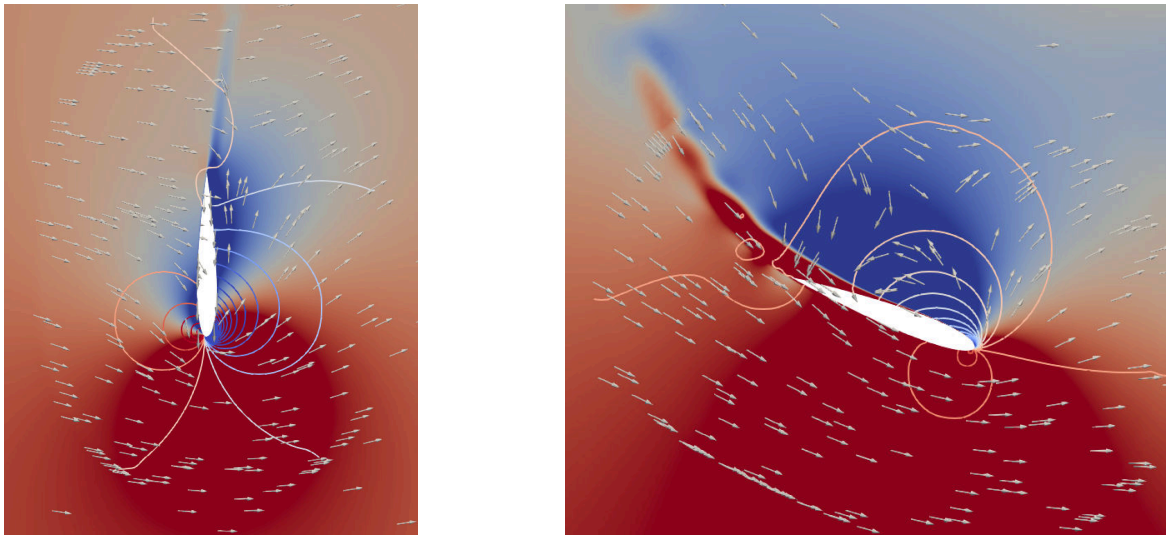

(a) (b)

Figure 13. Flow around a blade with $c = 0.04$m and $\lambda = 4$ in translation (a) and during the rotation around the lower pulley (b). Absolute flow velocity in the streamwise direction re-scaled from 0 to U_∞ and iso-pressure lines are represented.

5. Conclusion

The bi-axial turbine seems to be an interesting way to achieve high efficiencies, potentially higher than those of a conventional Darriues turbine. In the kinematics studied here, the blades have two points of contact with the chain, one close to the leading edge and the other close to the trailing edge. This avoids discontinuities in blade rotation speed. The use of an overset type mesh to impose the kinematics of the blade is an extremely flexible solution. The numerical simulation process has been validated by comparison with experimental and numerical data of an oscillating airfoil case. This study allowed to highlight the impact of the solidity parameter on 1-blade turbines. It appears that by decreasing the blade size, the optimal λ increases and the C_p max as well as the amplitude of discontinuities of C_p at the entry of the turns decrease. Subsequently, a study of the impact of the number of blades on turbine performance will be conducted.

References

[1] M. Worstell, "Aerodynamic Performance of the DOE/Sandia 17-m Diameter Vertical Axis Wind Turbine," Journal of Energy, p. 39–42, 1981.

[2] J. Dabiri, "Potential order-of-magnitude enhancement of wind farm power density via counter-rotating vertical-axis wind turbine arrays," Journal of Renewable and Sustainable Energy, vol. 3, no. 4, p. 043104, 2011.

[3] H. Sutherland, D. Berg, and T. Ashwill, "A Retrospective of VAWT Technology," Tech. Rep. SAND2012-0304, SANDIA, 2012.

[4] V. Clary, T. Oudart, P. Larroudé, J. Sommeria, and T. Maître, "An optimally-controlled RANS Actuator force model for efficient computations of tidal turbine arrays," Ocean Engineering, vol. 212, p. 107677, 2020.

[5] G. Naccache and M. Paraschivoiu, "Development of the dual vertical axis wind turbine using computational fluid dynamics," Journal of Fluids Engineering, vol. 139, 2017.

[6] F. Menter, "Two-Equation Eddy-Viscosity Turbulence Models for Engineering Applications," AIAA Journal, vol. 32, p. 1598–1604, August 1994.

[7] T. Lee and P. Gerontakos, "Investigation of flow over an oscillating airfoil," Journal of Fluid Mechanics, vol. 512, pp. 313–341, 2004.

[8] P.-L. Delafin, T. Nishino, A. Kolios, and L. Wang, "Comparison of low-order aerodynamic models and rans cfd for fullscale 3d vertical axis wind turbines," Renewable Energy, vol. 139, 2017.

[9] P.-L. Delafin, T. Nishino, L. Wang, and A. Kolios, "Effect of the number of blades and solidity on the performance of a vertical axis wind turbine," Journal of Physics: Conference Series, vol. 753, p. 022033, sep 2016.